An intrinsic lipid-binding interface controls sphingosine kinase 1 function

Michael J. Pulkoski-Gross, Meredith L. Jenkins, Jean-Philip Truman, Mohamed F. Salama, Christopher J. Clarke, John E. Burke, … & Lina M. Obeid

March 2018

An intrinsic lipid-binding interface controls sphingosine kinase 1 function[S]

Michael J. Pulkoski-Gross,*,† Meredith L. Jenkins,§ Jean-Philip Truman,† Mohamed F. Salama, Christopher J. Clarke,† John E. Burke,§ Yusuf A. Hannun,† and Lina M. Obeid[1,†,††]**

Department of Pharmacological Sciences,* and Department of Medicine and Stony Brook Cancer Center,† Stony Brook University, Stony Brook, NY 11790; Department of Biochemistry and Microbiology,§ University of Victoria, Victoria, British Columbia V8N 1A1, Canada; Department of Biochemistry,** Faculty of Veterinary Medicine, Mansoura University, Mansoura 35511, Egypt; and Northport Veterans Affairs Medical Center,†† Northport, NY 11768

Abstract Sphingosine kinase 1 (SK1) is required for production of sphingosine-1-phosphate (S1P) and thereby regulates many cellular processes, including cellular growth, immune cell trafficking, and inflammation. To produce S1P, SK1 must access sphingosine directly from membranes. However, the molecular mechanisms underlying SK1's direct membrane interactions remain unclear. We used hydrogen/deuterium exchange MS to study interactions of SK1 with membrane vesicles. Using the CRISPR/Cas9 technique to generate HCT116 cells lacking SK1, we explored the effects of membrane interface disruption and the function of the SK1 interaction site. Disrupting the interface resulted in reduced membrane association and decreased cellular SK1 activity. Moreover, SK1-dependent signaling, including cell invasion and endocytosis, was abolished upon mutation of the membrane-binding interface. Of note, we identified a positively charged motif on SK1 that is responsible for electrostatic interactions with membranes. Furthermore, we demonstrated that SK1 uses a single contiguous interface, consisting of an electrostatic site and a hydrophobic site, to interact with membrane-associated anionic phospholipids. Altogether, these results define a composite domain in SK1 that regulates its intrinsic ability to bind membranes and indicate that this binding is critical for proper SK1 function. This work will allow for a new line of thinking for targeting SK1 in disease.—Pulkoski-Gross, M. J., M. L. Jenkins, J-P. Truman, M. F. Salama, C. J. Clarke, J. E. Burke, Y. A. Hannun, and L. M. Obeid. **An intrinsic lipid-binding interface controls sphingosine kinase 1 function. *J. Lipid Res*. 2018.** 59: **462–474.**

Supplementary key words sphingolipids • sphingosine-1-phosphate • hydrogen-deuterium exchange mass spectrometry • enzyme regulation • cell signaling

Sphingosine kinase 1 (SK1) is a critical enzyme in the sphingolipid metabolic pathway as it can modulate the balance between the pro-apoptotic lipids, sphingosine (Sph) and ceramide, and the pro-survival and pro-inflammatory lipid, sphingosine-1-phosphate (S1P). S1P can signal in two distinct ways, either through binding to one of five S1P-specific G protein-coupled receptors, or as an intracellular second messenger, although the latter is not a well-understood mechanism. S1P and its producing enzymes have been implicated in a host of biological and pathophysiological roles, including cancer biology, inflammation, immune responses, vascular biology, and many others (1–5).

SK1 is upregulated in several cancers, including colon (6), lung (7), kidney (8), and brain cancers (9). SK1 expression has been correlated with poor prognosis and survival in patients (9–11). SK1 and S1P have been associated with increased proliferation, survival, and resistance to chemotherapy (12–14). Furthermore, SK1 has been implicated in inflammatory diseases, such as inflammatory bowel disease (15, 16), which is now thought to be an underlying

This work was supported by National Cancer Institute Grant F31CA196315 (National Research Service Award to M.J.P-G.), a new investigator grant to J.E.B. from Canadian Institutes of Health Research, Natural Sciences and Engineering Research Council of Canada Grant NSERC-2014-05218, a US Department of Veterans Affairs Merit Award (L.M.O.), National Institute of General Medical Sciences Grant GM06 GM097741 (L.M.O.), and National Institutes of Health Grant P01 CA097132 (L.M.O., Y.A.H.). The content is solely the responsibility of the authors and does not necessarily represent the official views of the National Institutes of Health.

Manuscript received 18 October 2017 and in revised form 4 January 2018.

Published, JLR Papers in Press, January 11, 2018
DOI https://doi.org/10.1194/jlr.M081307

Abbreviations: C17, 17 carbon; CIB1, calcium/integrin binding protein 1; CTD, C-terminal domain; CV, column volume; DOPA, 1,2-dioleoyl-*sn*-glycero-3-phosphate; DOPC, 1,2-dioleoyl-*sn*-glycero-3-phosphocholine; DOPE, 1,2-dioleoyl-*sn*-glycero-3-phosphoethanolamine; DOPS, 1,2-dioleoyl-*sn*-glycero-3-phospho-L-serine; ERM, ezrin-radixin-moesin; EV, empty vector; HDX, hydrogen/deuterium exchange; indel, insertion/deletion; MβCD, methyl-β cyclodextrin; NTD, N-terminal domain; PA, phosphatidic acid; PBST, PBS with Tween 20; PC, phosphatidylcholine; PE, phosphatidylethanolamine; PG, phosphatidylglycerol; PI, phosphatidylinositol; PLD, phospholipase D; PS, phosphatidylserine; SK1, sphingosine kinase 1; S1P, sphingosine-1-phosphate; Sph, sphingosine.

[1]To whom correspondence should be addressed.
e-mail: lina.obeid@stonybrookmedicine.edu

[S] The online version of this article (available at http://www.jlr.org) contains a supplement.

factor for cancer development and progression. While there is a plethora of knowledge about the biology of S1P and SK1, there is relatively little known about the molecular mechanisms that regulate its function.

SK1 has been shown to translocate to the plasma membrane after stimulation with PMA (17–19). Additionally, SK1 has been shown to have increased activity in membrane bound fractions from cells and that it can be activated in vitro by the phospholipids, phosphatidylserine (PS) and phosphatidic acid (PA), which are found in membranes (20, 21). Additionally, it was shown that SK1 was an effector of PA in cells (22). There are currently three different proposed mechanisms to explain SK1 translocation and interaction with membranes. Two of the mechanisms identify certain residues that mediate membrane localization (21, 23), while the third explains SK1 localization as being dependent on another protein, calcium/integrin binding protein 1 (CIB1) (24, 25). Interestingly, the protein-protein interaction between SK1 and CIB1 takes place at a hydrophobic site on SK1, which has been identified for membrane interaction. The residues identified by Stahelin et al. (21), Thr54 and Asn89, were proposed to interact with PS in the membrane. On the other hand, the residues identified by Shen et al. (23) are part of a small hydrophobic patch on the surface of SK1, and these authors implicated these residues in mediating endocytosis and neurotransmission.

In this work, we identify a missing piece of the SK1 translocation puzzle as a small highly positively charged three-residue motif near the active site. Evidence is provided for a contiguous membrane interaction surface consisting of both the electrostatic and hydrophobic sites. Furthermore, the results reveal that both the previously identified hydrophobic patch and the newly identified electrostatic motif are both essential for allowing SK1 binding to membranes in vitro and in cells. The results demonstrate that this positively charged site is important for mediating SK1 signaling processes, including cell invasion and colocalization with N-bar proteins during endocytosis. Overall, we propose a dual-site mechanism along a contiguous surface interface, which controls the interaction between SK1 and membranes. Importantly, disruption of either site or the combined disruption of both sites is sufficient to disrupt SK1-membrane interactions and SK1 signaling.

MATERIALS AND METHODS

Materials

Lipids including 1,2-dioleoyl-*sn*-glycero-3-phosphocholine (DOPC), 1,2-dioleoyl-*sn*-glycero-3-phosphate (DOPA), 1,2-dioleoyl-*sn*-glycero-3-phospho-L-serine (DOPS), 1,2-dioleoyl-*sn*-glycero-3-phospho-(1′-rac-glycerol) (DOPG), 1,2-dioleoyl-*sn*-glycero-3-phosphoethanolamine (DOPE), 1,2-dioleoyl-*sn*-glycero-3-phospho-(1′-myo-inositol) (DOPI), Sph, and S1P were purchased from Avanti Polar Lipids (Alabaster, AL). Monoclonal SK1, Na/K ATPase, phospho-ezrin-radixin-moesin (ERM), and t-ezrin antibodies were purchased from Cell Signaling Technologies (Danvers, MA). Tubulin antibody was purchased from Sigma-Aldrich (St. Louis, MO).

In silico analysis of SK1

Hydrophobicity and electrostatic potential maps were plotted on a surface representation (Protein Data Bank identification number 3VZB) using Chimera software (26). The molecule was prepared by adding hydrogen atoms and assigning atomic charge and radii through the PDB2PQR tool (27, 28) in Chimera, which uses parameters optimized for Poisson-Boltzmann calculations. Electrostatic and hydrophobic potentials were calculated with the Adaptive Poisson-Boltzman Solver (29) through the web service provided by the National Biomedical Computational Resource and the Kyte-Doolittle scale of hydrophobicity (30), respectively. Chimera software was used to generate cartoon representations of SK1.

Protein expression and purification

Insect cells ($2–3 \times 10^6$ cells/ml) were infected with bacculovirus expressing His_6-tagged SK1 constructs made using the Bac-to-Bac protocol (Invitrogen). After 72 h, cells were harvested and resuspended in lysis buffer [50 mM Tris (pH 8.5), 5 mM β-mercaptoethanol, 100 mM NaCl, 5 mM phenylmethyl sulfonyl fluoride, 1% Tween 20, and a protease inhibitor cocktail tablet (Roche)]. Cells were sonicated and spun down at 58,000 *g* for 1 h at 4°C. Supernatant was run over a Ni^{2+}-NTA column. The column was washed with 10 column volumes (CVs) of buffer A [20 mM Tris (pH 8.5), 5 mM β-mercaptoethanol, 250 mM NaCl, 40 mM imidazole (pH 8), 0.1% Tween 20, and 10% glycerol], washed with 2 CVs of buffer B [20 mM Tris (pH 8.5), 5 mM β-mercaptoethanol, 1 M NaCl, 0.1% Tween 20, and 10% glycerol], and eluted in 5 CVs of buffer C [20 mM Tris (pH 8.5), 5 mM β-mercaptoethanol, 100 mM NaCl, 500 mM imidazole (pH 8), 0.1% Tween 20, and 10% glycerol]. Fractions with SK1 protein were pooled and run over a size exclusion column in SEC buffer [20 mM Tris (pH 8.5), 5 mM β-mercaptoethanol, 100 mM sodium chloride, 0.1% Tween 20, and 10% glycerol]. Protein was concentrated to >1 mg/ml using a spin column with a 10,000 Da molecular mass cutoff. Protein purified for hydrogen/deuterium exchange (HDX) experiments was purified as described above, but in Tris buffer (pH 7.0).

Lipid protein overlay

Five micrograms of lipid (in chloroform) were spotted onto nitrocellulose membrane and blocked for 1 h in 3% fatty acid-free BSA (Akron Biotech, Boca Raton, FL) in PBS with Tween 20 (PBST). WT or mutant protein (at a concentration of 1 μg/ml) in PBST was incubated overnight with shaking at 4°C. Primary and secondary antibodies (in 3% fatty acid-free BSA in PBST) were incubated for 1 h each with one 20 min wash in PBST in between each incubation and after the last incubation. For specificity overlays, different amounts of lipids were spotted onto nitrocellulose membranes and the same protocol was followed as above. Membranes were developed using standard chemiluminescence-based Western blotting.

Sphingosine kinase activity assay

Activity was measured by the production of a fluorescent S1P as previously described (31, 32).

Liposome generation and sedimentation assays

Liposomes were made by three rounds of freeze-thaw (−80° to room temperature) with agitation. This was followed by sonication in a water bath until a homogenous solution was achieved (~5 min), which generates small unilamellar liposomes (33). The mean sizes of these liposomes were estimated by nanoparticle tracking analysis with a ZetaView (Particle Metrix, Germany) with a diameter of ~70 nm. The pelleting efficiency of these liposomes

was calculated by measuring fluorescence of NBD-PE-labeled liposomes before and after centrifugation and was found to be 87 ± 6%. Liposomes were composed of 40% DOPC, 35% DOPE, 20% DOPA or DOPS, and 5% cholesterol at a final concentration of 1 mM in buffer containing 100 mM NaCl, 50 mM HEPES (pH 7.5), and 150 mM sucrose. Forty microliters of liposomes were mixed with 50 μl of 0.1 ug/ul protein [in 50 mM HEPES (pH 7.5) and 100 mM NaCl] and incubated at room temperature for 10 min. Liposomes were sedimented at 100,000 *g* for 1 h and supernatants were removed; pellets were solubilized in buffer and samples were analyzed by SDS-PAGE. Proteins were visualized by Coomassie Brilliant Blue staining. Image analysis was performed with ImageJ.

Generation of HCT116crSK1 cells using Crispr/Cas9 technology

To knockout SK1 from HC116 cells, we used the LentiCRISPR v2.0 system (34, 35). The LentiCRISPR v2 plasmid was a gift from Feng Zhang (Addgene plasmid #52961). Briefly, guide RNAs targeting the SK1 gene were designed using the ChopChop algorithm (http://chopchop.cbu.uib.no/) and cloned into the plasmid as described previously (34, 35). To generate lentivirus, plasmids were cotransfected with VSV-G and dVPR into 293T cells and virus-containing medium was harvested and filtered (0.22 um PVDF membrane) after 72 h. HCT116 cells (100,000) were infected with 1 ml virus in the presence of polybrene (8 ug/ml). After 48 h, cells were selected in puromycin (2 ug/ml) for 7 days. Subsequently, cells were maintained in normal growth medium. Validation of genetic modification was performed with the GeneArt genomic cleavage detection kit (Thermo Scientific) according to manufacturer's instructions.

Cell lines and transfection

HCT116 Vec and HCT116crSK1 cell lines were maintained in DMEM (Life Technologies) containing 10% FBS and HeLa cells were maintained in RPMI 1640 (Life Technologies) containing 10% FBS. Medium without serum was used for serum starvation. Cells were checked for mycoplasma contamination every 2 months using a mycoplasma detection kit (Lonza, Basel, Switzerland) as per the manufacturer's instructions. Transfections were carried out using X-tremeGene 9 (Roche, Basel, Switzerland) (3 ul of reagent per transfection) and 500 ng of each DNA construct. Transfections were allowed to incubate for 24 h before changing the medium.

Seventeen carbon Sph labeling

Cells were transfected for 24 h with SK1 constructs using X-tremeGene (Roche). At 24 h, the medium was changed followed by a 15 min incubation with 17 carbon (C17)-Sph (0.5 μM final concentration). Briefly, cells were harvested by scraping directly into ice-cold PBS. Cells were subsequently pelleted and the PBS was removed. Cells were resuspended in 2 ml of cell extraction buffer (70% isopropanol:ethyl acetate; 2:3) and vortexed. Extraction and analysis were performed as previously described (36).

Membrane fractionation

HCT116crSK1 cells transfected with SK1 constructs were scraped in 500 μl fractionation buffer [250 mM sucrose, 20 mM HEPES (pH 7.4), 10 mM potassium chloride, 1.5 mM magnesium chloride, 1 mM EDTA, and protease inhibitor cocktail (Sigma-Aldrich)] at 75–80% confluency. Cells were lysed by 20 passes through a 27 gauge needle. Lysates underwent differential centrifugations: 900 *g* for 5 min to remove nuclei, followed by centrifugation at 9,600 *g* for 10 min to remove mitochondria, followed by a final spin at 100,000 *g* for 1 h at 4°C to separate cytosol from membranes. The pellet present after the final spin was the membrane fraction. The pellet was resuspended in 1/10 the starting volume and solubilized by sonication. Protein concentration was determined by BCA (Pierce) and proteins were separated by SDS-PAGE and analyzed by Western blot.

Membrane localization

HEK293 cells were transfected with GFP-tagged SK1 constructs for 24 h using X-tremeGene (Invitrogen). After 24 h, the cells were serum starved for 4–6 h and stimulated with serum for 30 min. After serum stimulation, the cells were washed with PBS and fixed in 3.7% paraformaldehyde for 10 min. After fixation, the cells were washed for 5 min in PBS three times followed by addition of mounting medium containing the nuclear stain, DAPI. Imaging was performed on a Leica TCS SP8 scanning-laser confocal microscope.

Cell invasion assays

Twenty-four-well Matrigel-coated transwell invasion plates (Corning Life Sciences, Corning, NY) were used to assess the invasive capacity of HCT116crSK1 cells. Cells were transfected with pcDNA3 empty vector (EV) or pcDNA3 containing SK1 constructs for 24 h. Cells were then serum starved for 4 h prior to seeding in 24-well transwell plates. Five hundred microliters of full serum (10%) medium were placed in the bottom chamber as a chemoattractant, while 75,000 cells per well were seeded into the top chamber in serum-free medium. Plates were incubated for 48 h at 37°C and 5% CO_2. At 48 h, the cells that had invaded to the bottom of the transwell were stained with Calcein AM (Invitrogen) and fluorescence was read in a SpectraMax plate reader.

Methyl-β cyclodextrin treatment

HeLa cells were cotransfected with GFP-tagged SK1 constructs and with endophilin A2-Ruby construct (a generous gift from Dr. Pietro De Camilli, Yale University). Twenty-four hours after transfection, cells were serum starved overnight followed by treatment with 1× methyl-β cyclodextrin (MβCD) {a 5× starting stock of 66 mg/ml MβCD in imaging buffer [10 mM HEPES (pH 7.5), 120 mM sodium chloride, 2 mM calcium chloride, 2 mM magnesium chloride, and 3 mM potassium chloride]}. After a 2 min treatment, the cells were immediately washed with PBS and fixed in 3.7% paraformaldehyde for 10 min. Mounting medium was added and the cells were imaged. Imaging was performed on a Leica TCS SP8 scanning-laser confocal microscope.

HDX-MS

HDX reactions were prepared with 20 pmol SK1 in either a lipid-containing buffer [20 mM Tris (pH 7.0), 100 mM NaCl, 10% glycerol, 0.1% Tween 20, and 5 mM BME] or a liposome-containing buffer (40% DOPC, 35% DOPE, 20% DOPA, and 5% cholesterol) at a final concentration of 0.69 mg/ml. Liposomes for exchange experiments were made via extrusion through a 0.1 μm polycarbonate filter after three freeze-thaw cycles. Exchange was initiated by the addition of 39.8 μl of D_2O buffer solution [10 mM HEPES (pH 7.5), 50 mM NaCl, and 97% D_2O] to give a final concentration of 77% D_2O, following the incubation of protein with either the lipid-containing buffer or the liposome-containing buffer. Exchange was carried out for 3, 30, and 300 s, and exchange was terminated by the addition of a quench buffer (final concentration 0.6 M guanidine-HCl, 0.8% formic acid). Samples were rapidly frozen in liquid nitrogen and stored at −80°C until mass analysis.

Protein samples were rapidly thawed and injected onto a UPLC system at 2°C according to previously published protocols (37). The protein was run over two immobilized pepsin columns (Poroszyme,

2-3131-00; Applied Biosystems) at 10°C and 2°C at 200 μl/min for 3 min, and peptides were collected onto a VanGuard precolumn trap (Waters). The trap was subsequently eluted in line with an Acquity 1.7 μm particle, 100 × 1 mm^2 C18 UPLC column (Waters), using a gradient of 5–36% buffer B (buffer A, 0.1% formic acid; buffer B, 100% acetonitrile) over 16 min. MS experiments were performed on an Impact II TOF (Bruker) acquiring over a mass range from *m/z* 150 to 2,200 using an electrospray ionization source operated at a temperature of 200°C and a spray voltage of 4.5 kV. Peptides were identified using data-dependent acquisition methods following MS/MS experiments (0.5 s precursor scan from *m/z* 150 to 2,200; twelve 0.25 s fragment scans from *m/z* 150 to 2,200). MS/MS datasets were analyzed using PEAKS7 (PEAKS), and a false discovery rate was set at 1% using a database of purified proteins and known contaminants.

HD-Examiner software (Sierra Analytics) was used to automatically calculate the level of deuterium incorporation into each peptide. All peptides were manually inspected for correct charge state and presence of overlapping peptides. Deuteration levels were calculated using the centroid of the experimental isotope clusters. Changes in deuterium incorporation were considered significant for all changes between conditions >0.5 Da and 5% deuteration incorporation with $P < 0.05$ between triplicate samples.

Statistics

One-way or two-way ANOVA with Bonferroni post hoc tests or Student's *t*-test were used to assess statistical significance using GraphPad Prism 4 (La Jolla, CA) as appropriate. Statistical significance was defined as $P \leq 0.05$.

RESULTS

In silico surface binding analysis of SK1

The structure of SK1 (38) allowed for evaluation of the previously proposed mechanisms for SK1 interaction with membranes. Thr54, which was proposed by Stahelin et al. (21) to interact with PS, is in the β2-α2 loop and is important for interaction with ATP. Ans89, also proposed to interact with PS, is in the α3 helix and is involved in hydrogen bonding between the N-terminal domain (NTD) and C-terminal domain (CTD) of SK1. The hydrophobic residues identified by Shen et al. (23) (Leu194, Phe197, and Leu198; magenta residues **Fig. 1E**, F) are located on the protein surface, and could enhance interaction with membranes, but most likely nonspecifically, as this stretch does not allow SK1 to discriminate between neutral and charged lipids. Therefore, we conducted in silico surface electrostatic analysis using Chimera software (26) in order to reveal candidate residues that might mediate interactions with PS and PA. Electrostatic potentials were calculated using the Adaptive Poisson-Boltzman Solver in the Chimera software and were then mapped to a surface representation of SK1. On the surfaces shown in Fig. 1A, B, red-colored areas represent negatively charged surfaces, while blue-colored areas represent positively charged surfaces. A highly positively charged site composed of the residues Lys27, Lys29, and Arg186 (Fig. 1A, B, shown as blue surface) was identified on the surface of SK1. This electrostatic site (shown as blue residues in Fig. 1E, F) is adjacent to the substrate binding sites for both ATP and Sph. Additionally, surface hydrophobicity was also analyzed using Chimera software (Fig. 1C, D). Hydrophobic surfaces are represented by magenta-colored areas, while hydrophilic surfaces are represented by cyan-colored areas. The results showed the same hydrophobic site as that detected by Shen et al. (23), shown as magenta sticks in Fig. 1E, F. Importantly, a novel electrostatic site has been identified, which could mediate the interaction with PA and/or PS.

In vitro biochemical analysis of SK1 binding to anionic phospholipids and liposomes

Interestingly, the residues within the identified charged patch are more than 150 residues apart from each other, which makes it difficult to identify from the linear sequence. To disrupt this electrostatic site, Lys27 and Lys29 were mutated to glutamate residues and Arg186 to an aspartate residue (Triple-SK1), leaving the hydrophobic site intact. To disrupt the hydrophobic patch, Leu194 was mutated to a glutamine (L194Q-SK1), as described previously (23), leaving the electrostatic site intact. These mutants of SK1 were cloned into the pFastBac (Invitrogen) system for expression in and purification from insect cells. The mutation of these residues did not interfere with antibody (monoclonal antibody; Cell Signaling) recognition, as shown in supplemental Fig. S1A. Recombinant SK1 proteins (WT-SK1, L194Q-SK1, and Triple-SK1) were highly pure, as determined by SDS-PAGE (≥90%), as shown in **Fig. 2A**. Furthermore, these mutants are active in vitro, albeit they are less active than WT-SK1 (supplemental Fig. S1B).

First, the ability of WT-SK1 to discriminate between different anionic phospholipids was tested by employing a lipid-protein overlay assay. The results (supplemental Fig. S2) show that WT-SK1 was able to bind both PA and PS, with higher affinity for PA. WT-SK1 failed to bind to phosphatidylcholine (PC), phosphatidylglycerol (PG), or phosphatidylinositol (PI). Intriguingly, there was also weak binding to phosphatidylethanolamine (PE), which has a very similar head group to PS, but with a net neutral charge (supplemental Fig. S2). Next, WT-SK1 and mutant constructs were compared for their ability to bind to PA, PC, PS, or PE (Fig. 2B). L194Q-SK1 had reduced ability to bind PA, whereas the Triple-SK1 mutant was severely deficient in PA binding. Spot intensity for the protein-lipid overlays were quantified using ImageJ software (Fig. 2C). SK1 could discriminate between different anionic phospholipids (i.e., bound to PA and PS, but not to PC, PG, or PI). Furthermore, the electrostatic site was responsible for binding to PA, as mutation of the electrostatic site, but not mutation of the hydrophobic site, severely reduced binding to PA.

To evaluate SK1 binding in solution, we employed liposome sedimentation assays using multilamellar liposomes composed of PC/PE/cholesterol and either PA or PS (Fig. 2D). To characterize these liposomes, we evaluated size distribution as well as pelleting efficiency (shown in supplemental Fig. S1). WT-SK1 bound strongly to liposomes containing PA (~90% bound, Fig. 2E) and, similar to the lipid overlay results, there was weaker binding to PS-containing liposomes (~50% bound, Fig. 2E). Very little SK1

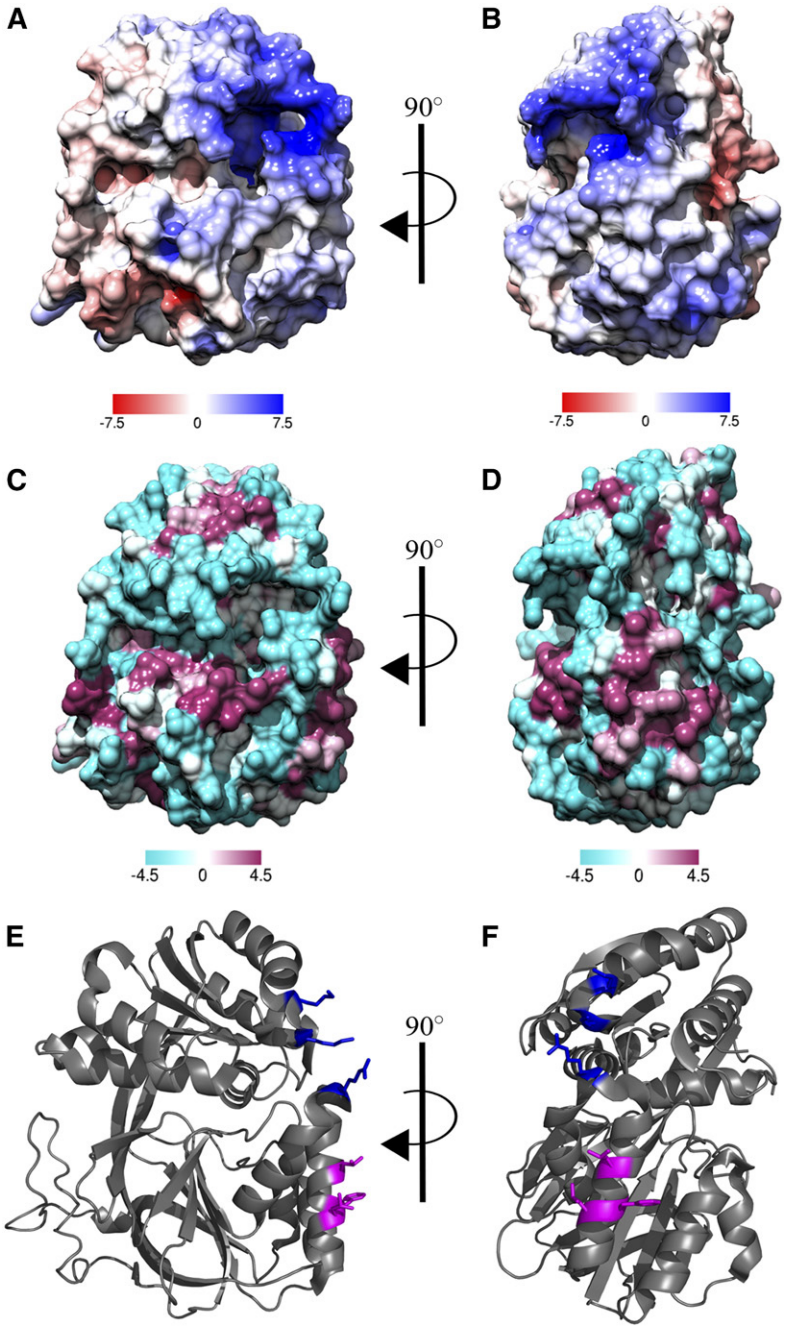

Fig. 1. In silico surface binding analysis of SK1. A and B: Electrostatic potential maps were generated using Chimera software using the Adaptive Poisson-Boltzman Solver. The scale represents kcal·mol^{-1} where blue represents positively charged areas and red represents negatively charged areas. C and D: The Kyte-Doolittle scale of hydrophobicity was used to predict hydrophobicity and was mapped to the surface of SK1 where cyan represents hydrophilic areas and magenta represents hydrophobic areas. E and F: Cartoon representation of SK1 with residues of the hydrophobic patch and electrostatic patch represented as magenta and blue sticks, respectively. Protein Data Bank identification number 3VZB (38) used for all analyses.

bound to the control liposomes containing PC/PE/cholesterol (Fig. 2D, E). When either L194Q-SK1 or Triple-SK1 was analyzed for membrane binding, both were found to be almost exclusively in the supernatant (<10% bound, Fig. 2D, E). These results indicated that both sites are critical for binding to membranes containing certain anionic phospholipids and that disruption of either can be detrimental to SK1 membrane binding.

Mapping of SK1/liposome interface with HDX-MS

To characterize the interactions of SK1 with membrane vesicles, we employed HDX-MS (**Fig. 3**). This is a powerful analytical technique that measures the exchange rate of amide hydrogens with solvent. Protection from amide exchange is mediated by involvement in secondary structure, and measuring exchange rates allows determination of protein conformational dynamics. This technique has been deployed to probe the interaction of lipid-modifying enzymes with membranes and membrane proteins (37, 39–42). SK1 was incubated in the presence and absence of membrane vesicles composed of 40% PC, 35% PE, 20% PA, and 5% cholesterol. HDX-MS experiments were carried out for three time points (3, 30, and 300 s) for both conditions. All peptides identified and analyzed for all experiments, along with their deuteration states, are listed in supplemental Fig. S3.

Large decreases in HDX were apparent in a single contiguous surface of both the NTD and CTD of SK1 (Fig. 3A). SK1, in the absence of any membranes, showed no protection in the α7 and α8 helices, indicating that they contain

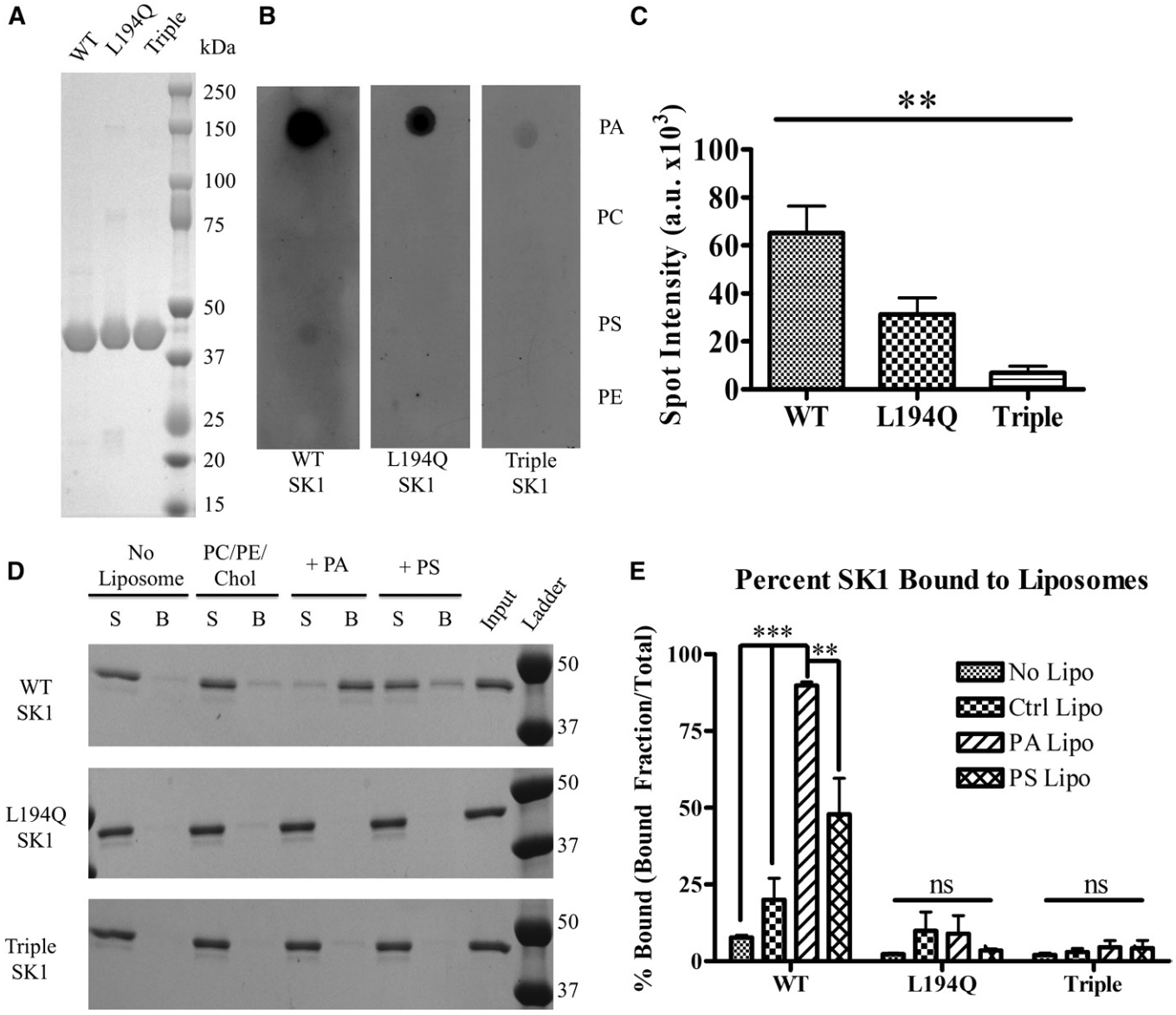

Fig. 2. In vitro binding analysis of SK1 WT and SK1 mutants. A: SDS-PAGE analysis of purified SK1 proteins. B: Protein-lipid overlay comparing the ability of WT versus mutant to bind to PA, PC, PS, or PE. C: Quantification of B using densitometry (ImageJ). Data represent the mean ± SD of n = 3; $^{**}P < 0.01$ as per one-way ANOVA. D: Liposome sedimentation assay with liposomes containing PC, PE, cholesterol (Chol), and either PA or PS (representative image of n = 3). E: Quantification of D using Image J. Data represent the mean ± SD of n = 3; $^{**}P < 0.01$, $^{***}P < 0.001$ as per a two-way ANOVA.

either no or very transient secondary structure. However, the largest decreases in exchange upon membrane binding, by far, were apparent in the same region stretching from amino acid 167 to amino acid 197 (encompassing the α7 and α8 helices, Fig. 3B). This is indicative of a disorder-order transition upon membrane binding. Large conformational changes upon lipid binding had been discovered in this region using X-ray crystallography (38) and is consistent with the proposed model of α7 and α8 acting as a lid over the active site (43). Importantly, this region contains Arg186 of the electrostatic patch and Leu194 of hydrophobic patch. There were also large decreases in exchange in the α9 helix (peptides 289-299 and 303-313, Fig. 3B) upon membrane binding, consistent with the previous annotation of this region as participating in lipid binding. There were also smaller, but significant, decreases in exchange in the NTD, with decreases at the β1 α1 elements (peptides 18-33, Fig. 3B), as well as at α5 (peptides 117-125, Fig. 3B). The β1 α1 region (containing Lys27 and Lys29 of the electrostatic motif, Fig. 3A) is located on the putative membrane binding face of the NTD, and is located directly opposite the α7 α8 region. Furthermore, there was a decrease in exchange at the C-terminal section of the α5 helix. Additionally, a decrease in exchange at the C terminus and β17 region (peptides 360-385, with the majority of the difference localized in the region from peptide 360 to peptide 365; Fig. 3B, supplemental Fig. S3) was also observed. Structurally, the C terminus lies directly over the α5 helix and may contribute in the regulation of SK, as previously noted (43). Membrane binding induced changes in deuterium

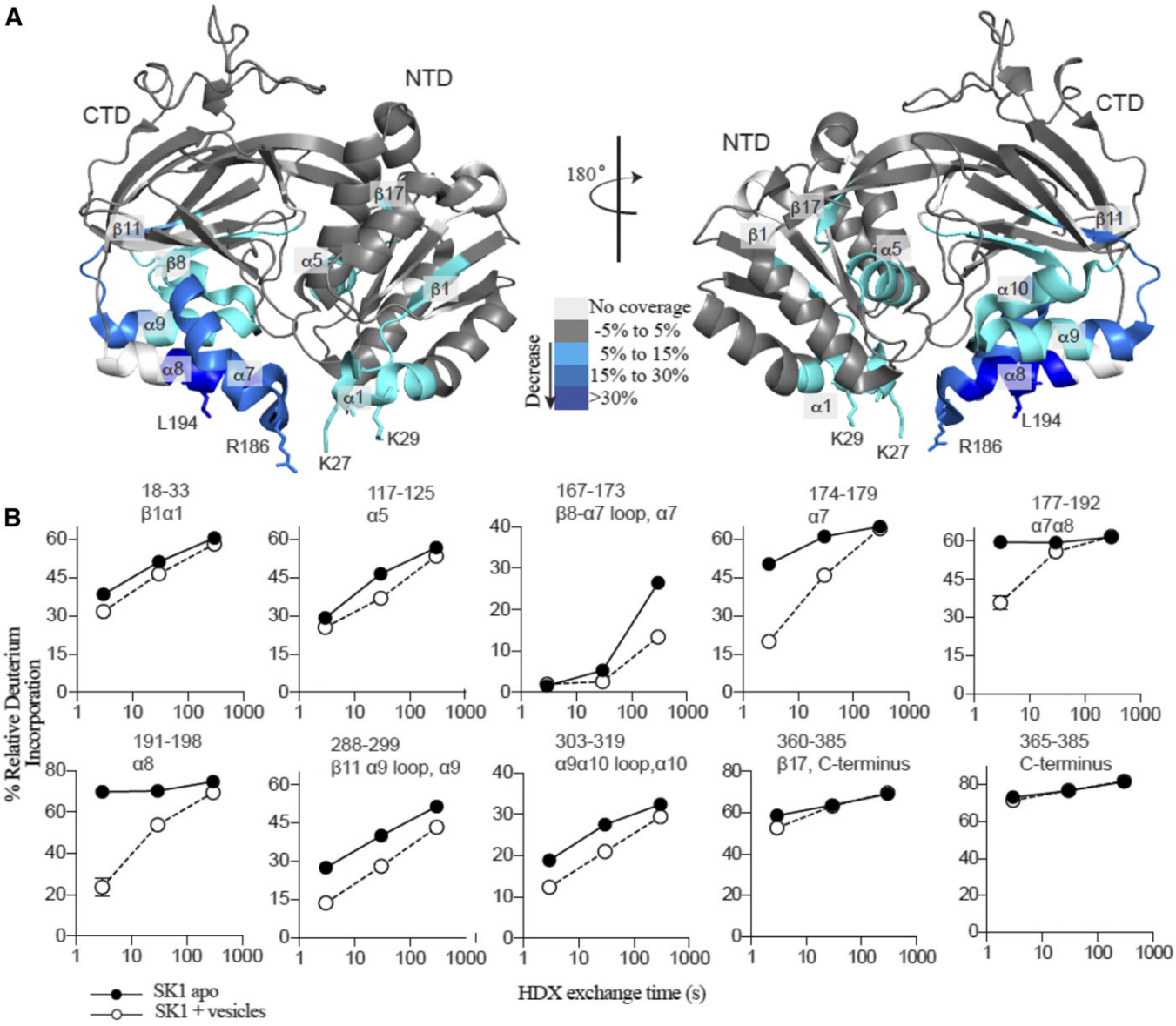

Fig. 3. HDX-MS characterizes changes induced by SK1 membrane binding. A: Peptides that showed deuterium exchange differences greater than 5% and 0.5 Da between the apo state and membrane bound states of SK1 are mapped according the legend on the crystal structure of SK1 (Protein Data Bank identification number 3VZB) (38). Residues mutated in this study are shown as sticks and labeled. Secondary structure annotations are labeled on the structure. B: Time course of deuterium incorporation for a selection of peptides that showed significant differences in percent deuteration upon the addition of membrane (error shown as SD; n = 3). The full set of deuterium incorporation data is shown in supplemental Fig. S3.

incorporation into SK1 peptides, including peptides spanning the electrostatic and hydrophobic sites. These two sites align to form a single contiguous membrane binding interface.

Loss of membrane binding in cells

In order to test these mutants in cells, it became important to express them in the absence of endogenous WT-SK1. Therefore, we generated HCT116 CRISPR SK1 (HCT116crSK1) cells using CRISPR/Cas9 technology. These cells were probed by Western blot, revealing that there was no detectable SK1 protein compared with the vector control cells (**Fig. 4A**). Furthermore, we used a genomic cleavage assay where DNA is cleaved at insertion/deletion (indel) regions (using the GeneArt genomic modification detection assay; Life Technologies). In the HCT116crSK1 cells, smaller DNA fragments were observed, indicating that genomic modification, specifically indels, has occurred in these cells and not in the vector control cells (Fig. 4B). Finally, we functionally confirmed that SK1 was removed by measuring endogenous sphingolipids of the HCT116crSK1 cells compared with the vector control cells. Both Sph and dihydrosphingosine levels were elevated in the crSK1 cells compared with the vector control, and S1P and dihydrosphingosine-1-phosphate levels were decreased (Fig. 4C, D).

Using the HCT116crSK1 cells, SK1 association with membranes was evaluated. We overexpressed either WT,

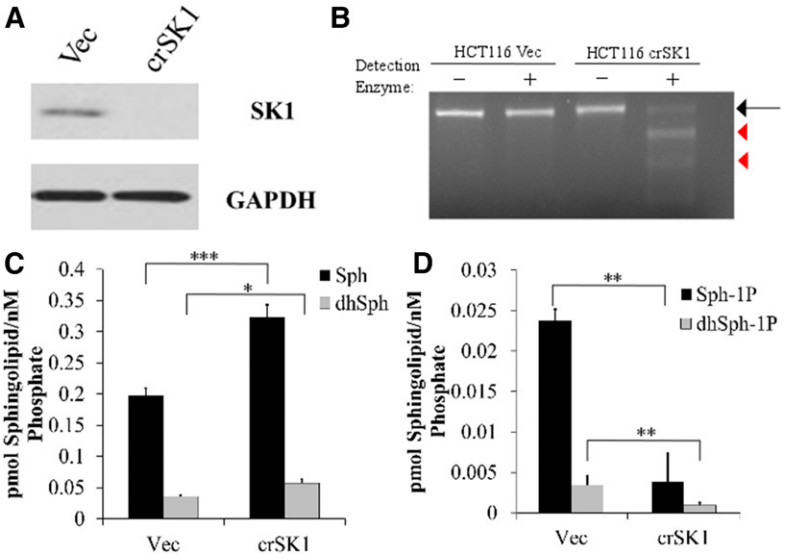

Fig. 4. Validation of HCT116 SK1 CRISPR cells. A: Immunoblot analysis of SK1 protein levels in vector control and CRISPER SK1 (crSK1) cells. B: GeneArt genomic cleavage detection assay (Life Technologies) used to detect small indels in the genome of the cells with CRISPR for SK1. The black arrow indicates the PCR product and the red arrowheads denote cleavage products. C: Sph and dihydro-Sph (dhSph) measurements of CRISPR and control cells increase in both species of lipids. D: Decreased S1P (Sph-1P) and dihydro S1P (dhSph-1P) measurements in the CRISPR cells. Lipid measurements are the mean ± SD of n = 3; $*P < 0.05$, $**P < 0.01$, $***P < 0.001$ as per paired Student's *t*-test.

L194Q, Triple, or a combination of both the Triple and L194Q mutant (T+L) constructs and fractionated the cells. When probed for SK1 using the monoclonal antibody (Cell Signaling), which recognizes all the mutants, the results showed that there was less SK1 associated at the membrane in the L194Q- and Triple-SK1 transfected cells compared with the WT in serum-starved conditions (**Fig. 5A**). The most striking loss of membrane association occurred when the two mutated sites were in the same construct, the T+L-SK1 mutation, resulting in more than a 67% decrease in the ratio of membrane-bound SK1 to cytosolic SK1 (Fig. 5A).

Next, it became important to determine the effects of membrane binding on SK1 activity in cells. SK activity in cells can be monitored by MS via the conversion of 17C-Sph to 17C-S1P (36). When WT-SK1 was overexpressed, there was a significant increase in C17-S1P, as compared with HCT116crSK1 cells transfected with EV (Fig. 5B). However, in the case of the overexpression of membrane binding mutants, the increase observed in the WT was diminished. When the two mutations were combined, this loss of C17-S1P generation was decreased further (Fig. 5B). The residual C17-S1P activity is likely due to the presence of SK2 in these cells. The overexpression of these mutants

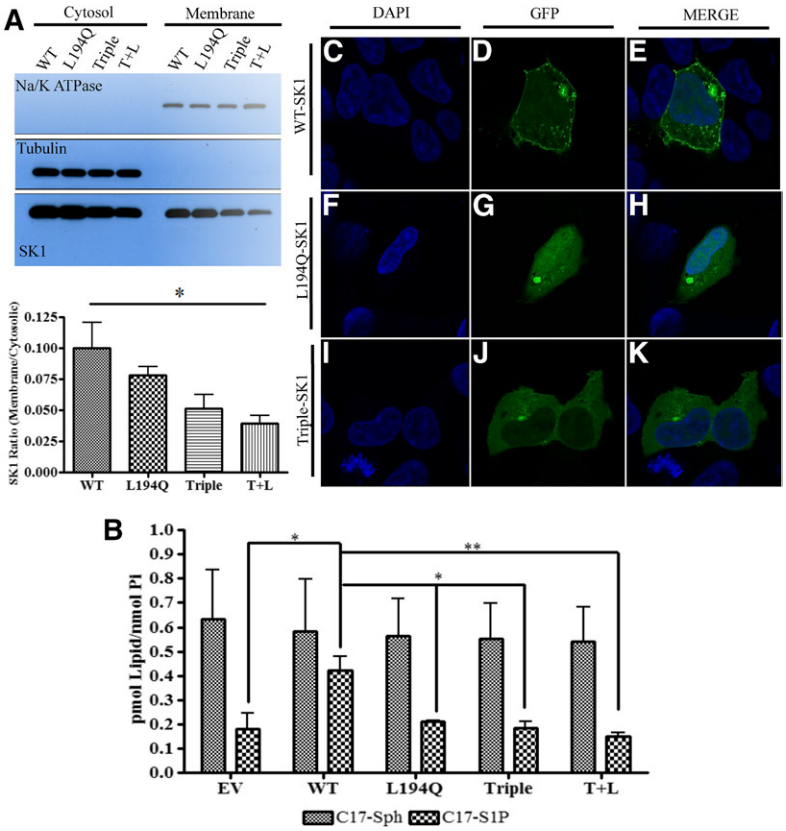

Fig. 5. Effects of SK1 membrane binding mutants in cells. A: Biochemical cell fractionation of HCT-116crSK1 cells overexpressing SK1 constructs. Cytosol was separated from membranes using ultracentrifugation. Quantification of the membrane to cytosolic ratio using ImageJ. Data represent the mean ± SD for three independent replicates. $*P < 0.05$ as per one-way ANOVA. B: C17-Sph labeling of HCT116crSK1 cells expressing EV, WT, L194Q, Triple, or T+L mutants. Data represent the mean ± SD of three independent experiments. $*P < 0.05$; $**P < 0.01$. C–K: HEK293 cells expressing GFP-tagged SK1 (WT, L194Q, or Triple) stimulated with 10% FBS. The nuclei of the cells were stained with DAPI. Representative images of three independent experiments.

did not affect uptake of C17-Sph, as shown by the cellular levels of C17-Sph (Fig. 5B). These data indicate that SK1 activity requires membrane binding, mediated by the two identified sites.

SK1 localization at the plasma membrane in HEK293 cells was also evaluated using confocal microscopy in HEK293 cells expressing GFP-tagged SK1 constructs (Fig. 5C–K). In cells expressing WT-SK1, SK1 was localized at the plasma membrane after stimulation with medium containing 10% FBS. However, under the same conditions, the L194Q- and Triple-SK1 mutations were unable to associate with the plasma membrane with serum stimulation. Therefore, mutation of either of the two sites can disrupt SK1 association with membranes.

Requirement of SK1 membrane binding for SK1 signaling and biology

To determine whether mutation of SK1's membrane binding interface influenced SK1 signaling processes, we used MβCD to sequester cholesterol and induce endocytosis. Shen et al. (23) showed that WT-SK1 could colocalize with the N-bar protein, endophilin-2, in response to membrane perturbations with either MβCD or sphingomyelinase treatment. In agreement with previous data, GFP-tagged WT-SK1 colocalized with Ruby-tagged endophilin-2 at membrane invaginations upon treatment with MβCD (**Fig. 6A**). Importantly, mutation of either the electrostatic site or the hydrophobic site was sufficient to disrupt this colocalization of SK1 and endophilin-2 (Fig. 6B, C). Combination of the two sites did not enhance the observed loss of colocalization (Fig. 6D), indicating that both sites are necessary for membrane binding in a biological setting.

To assess whether membrane binding affected SK1-dependent cell biology, we employed two different assays. We had previously shown that the phosphorylation of the ERM family of proteins upon treatment with exogenous Sph was dependent on SK1 (44). Indeed, using the CRISPR-mediated deletion of SK1, we now show that there was no significant ERM protein phosphorylation after treatment with exogenous Sph in the HCT116crSK1 cells transfected with EV (Fig. 6E). On the other hand, the response to S1P, which bypasses the requirement for SK1, was maintained. When WT-SK1 was overexpressed, it rescued the phenotype, showing that exogenous Sph addition induced phosphorylation of ERM proteins. Disruption of either the electrostatic or hydrophobic sites individually did not result in a dramatic loss of ERM phosphorylation (Fig. 6E). Interestingly, when the two mutants were combined (both sites mutated in the same construct), there was almost complete loss of ERM phosphorylation (Fig. 6A). These data suggest that disruption of the membrane interface can disrupt S1P-induced ERM phosphorylation.

Because ERM proteins are involved in cell motility, migration, and invasion, we evaluated invasion of the HCT116crSK1 cells using a Matrigel-coated transwell assay. The results showed that these HCT116crSK1 cells invaded through the Matrigel more efficiently when WT-SK1 was overexpressed, compared with EV. Strikingly, when overexpressing either the electrostatic mutant, hydrophobic mutant, or the two mutants combined, invasion was completely reduced to EV levels (Fig. 6F). This suggests that SK1's membrane binding is important for enhancing invasion and that disruption of membrane binding can have negative consequences for the functions of SK1.

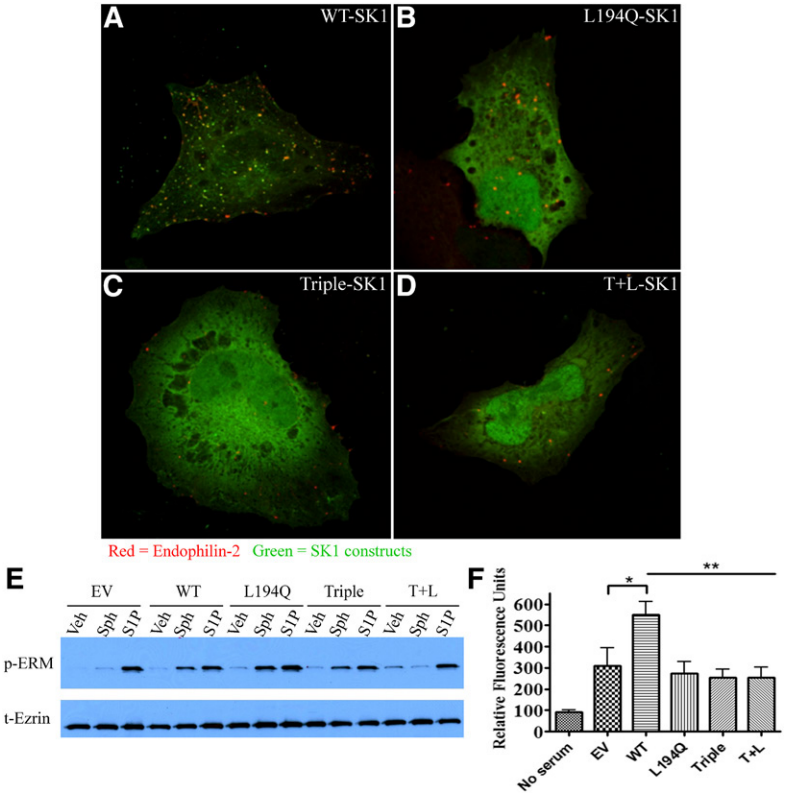

Fig. 6. Biological consequences of loss of membrane binding for SK1. A–D: Representative images of HeLa cells coexpressing GFP-SK1 (green) constructs and Endophilin2-Ruby (red). Colocalization was assessed after 2 min of treatment with MβCD. All experiments are n = 3. E: Effect of SK1 mutation on ERM phosphorylation upon addition of exogenous Sph (2.0 μM) or S1P (200 nM). F: Effect of SK1 mutation of the ability of HCT116crSK1 cells to invade through Matrigel. Cells were transfected with either EV or SK1 constructs and allowed to invade through Matrigel-coated membranes (8.0 μm pore size). $*P < 0.05$, $**P < 0.01$, as per one-way ANOVA; n = 3; error bars represent SD.

DISCUSSION

For more than two decades, SK1 and its pleiotropic lipid product, S1P, have been studied and implicated in cancer (1), inflammation (3), and development (45), yet, only recently have strides been made in understanding SK1 structure, function, and regulation. Even so, the mechanisms underlying SK1's interactions with membranes, where it can access Sph and produce S1P, have remained unclear.

Here, we identify a new electrostatic motif of SK1 responsible for binding to certain anionic phospholipids. Furthermore, this electrostatic site works in conjunction with a previously identified hydrophobic patch to bind to membranes. To map the membrane binding interface, we used HDX-MS to show that these two sites comprise a single contiguous interface. Cellular studies demonstrate that mutation of the two sites causes decreased membrane association and SK1 activity. Importantly, disrupting this interface results in loss of function for SK1-dependent cell invasion and SK1's role in endocytosis.

Our data suggest that SK1 uses an intrinsic single contiguous interaction interface (**Fig. 7C**) to associate with membranes. The contiguous site consists of two adjacent regions on the surface of SK1, an electrostatic region (colored blue in Fig. 7A–C) and a hydrophobic region (colored magenta in Fig. 7A–C). Our data show that the newly identified electrostatic site is equally as responsible for membrane association as the hydrophobic site, which indicates that SK1 requires both sites to be intact for optimal membrane binding. We speculate that this interaction might result in the partial insertion of the helices into the membrane (Fig. 7D). We thought about a different mechanism, where SK1 might partially extract lipids from the membrane, but this seemed to be the more unlikely scenario. Interestingly, membrane interaction along this contiguous surface leaves the 40-residue loop insertion in the catalytic domain, which contains Ser225 (Fig. 7D, red residue), exposed to the cytosol. Ser225 is known to be phosphorylated (19) and dephosphorylated (46, 47), making its exposure important for access by kinases and/or phosphatases. It is not clear how SK1 might exchange ATP when bound to the membrane, as membrane binding would mostly occlude the ATP binding site. Molecular dynamics simulations of SK1 and membranes would be beneficial to further our understanding of the effect of membrane binding on the catalytic cycle for SK1. Disruption of either of these two sites or the combined disruption of both sites was sufficient to result in loss of in vitro binding and cellular function, when looking at SK1-mediated signaling processes.

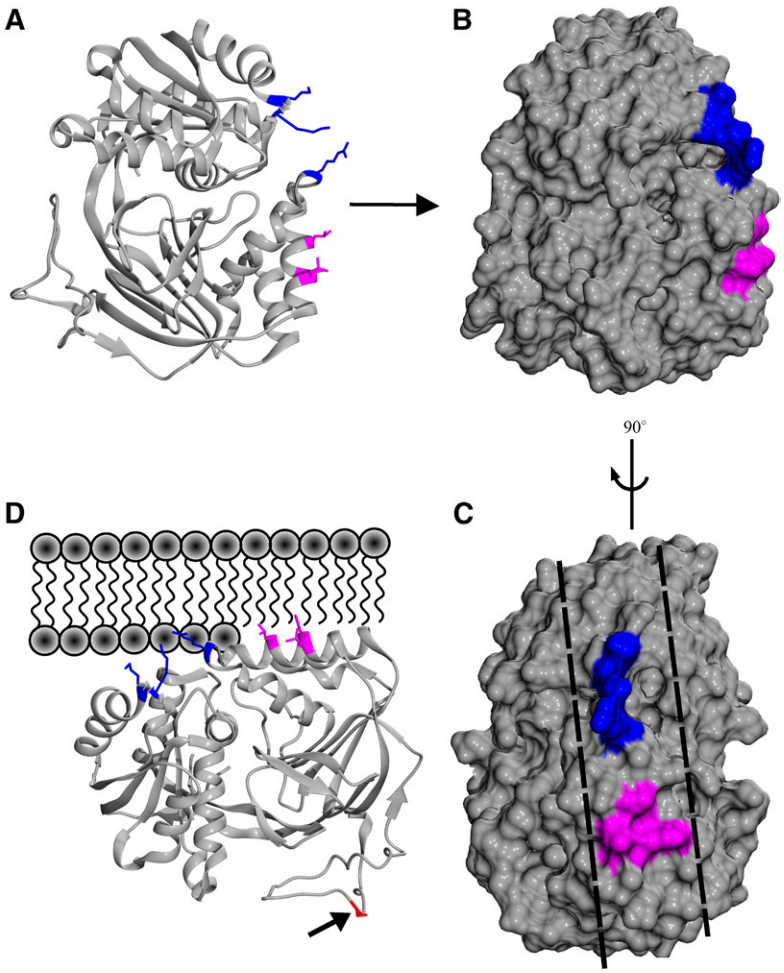

Fig. 7. Model of SK1 binding to membranes. A: Cartoon representations of SK1 showing the residues, as sticks, from the electrostatic patch (colored blue) and the hydrophobic patch (colored magenta). B: Surface representation of SK1 in the same orientation as A. The surface is colored according to A. C: Surface representation that is rotated approximately 90° relative to B and shows that these sites line up to form a single contiguous surface (dashed lines). D: Possible positioning of SK1 at a membrane interface to engage the single contiguous interaction interface (partially embedded in membrane) leaving Ser225 (arrow, red residue) accessible to cytosolic kinases/phosphatases.

SK1 has been shown to be activated in the presence of certain anionic phospholipids, such as PS and PA (20), and has been further defined as an effector of PA (22). The electrostatic site identified in this work provides a means by which SK1 can discriminate negatively charged lipids, such as PA, from neutral lipids, including PC and PE. Furthermore, the residues Thr54 and Asn89, which have been previously implicated in PS binding (21), showed no significant changes upon membrane binding in the HDX-MS experiments. This indicated that these residues do not play a direct role in the interaction with membranes, but it is possible that they play an indirect role. Furthermore, SK1 would potentially be able to extract Sph through membrane interaction with the helices (α7, α8, and α9) previously identified as important for membrane/lipid binding via assessing crystallographic data (38). Helices α7 and α8 have been shown to change position (via comparison of crystal structures) after lipid binding to the Sph binding pocket (38). Helices α9 and α10 (peptides 288-299 and 303-319) also showed protection from deuterium incorporation upon membrane binding. This result suggests a stabilization in their secondary structure after lipid binding or that there is a potential role for membrane interaction for substrate extraction; however, this remains to be seen. We speculate that interaction with cell membranes could induce the movement of these helices to promote binding of substrate and release of product.

An interesting component of the mechanism of many proteins that can bind membranes is their ability to sense curvature. It has been suggested that SK1 can sense the negative curvature of membranes (23). A mechanism has also been proposed in which SK1 can dimerize through interactions of the NTD of two protomers making a head-to-head homodimer complex (43). A recent study used computational analysis to better understand how SK1 might dimerize. Bayraktar, Ozkirimli, and Ulgen (48) suggest a putative dimerization interface that somewhat overlaps with the proposed mechanism of Adams, Pyne, and Pyne (43). Interestingly, a dimerization through the NTDs of two SK1 protomers would allow for the alignment of the interface identified in this work. This dimerization would have two implications: first, dimerization could allow for curvature sensing of SK1; and second, dimerization would allow for the strengthening of the interaction between SK1 and membranes. However, this putative dimer interface has yet to be confirmed biochemically or biophysically and requires further investigation.

Membrane localization of SK1 has also been attributed to interaction with CIB1 (24, 25), which acts as a calcium-myristoyl switch. Interestingly, this CIB1 interaction site, F197/L198 (24), overlaps with the hydrophobic patch that has been shown to be important for direct membrane binding in a previous study (23) and this work. As suggested by Jarman et al. (24), it is possible that CIB1 acts as a "molecular shepherd" to bring SK1 close enough to the membrane, but does not influence SK1's intrinsic mechanism for binding to membranes. However, it is also likely that CIB1 can "override" the intrinsic mechanism of SK1 membrane binding and force it to the membrane as a function of the myristoyl-switch. It is also possible that interaction with CIB1 is dependent on SK1 membrane interaction and mutation of the hydrophobic patch disrupts SK1 membrane binding and, subsequently, CIB1 interaction. Future work should be aimed at fully understanding the relationship between CIB1 and SK1 in SK1's translocation process.

Activity of membrane-associated SK1 has been documented in several studies (17, 49, 50). The C-terminal tail of SK1 has previously been shown to be important in regulating the activity of SK1 (51). It has since been postulated that the C-terminal tail of SK1 (specifically, residues 364-367) can act as a cap for the α5 helix, which extends into the catalytic site of SK1 (43). Our HDX-MS data show protection from exchange in the C-terminal tail of SK1 (mostly in residues 360-365) as well as the α5 helix upon membrane binding. It is possible that changes in the conformation of the C-terminal tail upon membrane binding could affect the capping/positioning of the catalytic residue, Asp81, indirectly through repositioning of the α5 helix, ultimately regulating SK1; however, this will require further study.

The role of SK1/S1P in cell biology and in disease has been well-documented and is reviewed in (1, 3, 52–54). We show that SK1's innate ability to bind to membranes is critical for the proper function of SK1 in invasion and its role in endocytosis. Our results also indicate that SK1 prefers to bind to PA in accordance with previous literature showing SK1 as an effector of PA in humans (22) and in *Arabidopsis thaliana* (55), and possibly suggesting conservation of SK1-PA binding. PA can be generated by the action of two different families of enzymes, phospholipase Ds (PLDs) or diacylglycerol kinases. A number of stimuli that activate PLD, such as platelet-derived growth factor (56), epidermal growth factor (57), and phorbol esters (58), are also known to activate and/or induce translocation of SK1 (17, 59, 60). Furthermore, PLD had been implicated in both clathrin-mediated and clathrin-independent endocytosis [reviewed in (61)]. Therefore, it will be interesting to fully comprehend the dynamic cross-talk between PA generation by PLD and/or diacylglycerol kinase and SK1 membrane association.

Overall, these data provide the first evidence of a complete interaction interface responsible for SK1 binding to membranes. It is also shown that membrane binding is critical for SK1-mediated biologies, including cell invasion and SK1's role in endocytosis. This work also opens new opportunities for studying allosteric mechanisms that might regulate SK1 function. Targeting this newly identified PA/PS binding motif might provide interesting avenues for inhibition of SK1 activity as a therapeutic option in cancer and/or inflammatory diseases.

The authors would like to thank the Lipidomics Facility of Stony Brook University for lipid analyses. The authors would also like to thank Janet Allopenna for her expertise and assistance with cloning and Dr. Pietro di Camilli for graciously providing the endophilin-2-Ruby construct.

REFERENCES

1. Heffernan-Stroud, L. A., and L. M. Obeid. 2013. Sphingosine kinase 1 in cancer. *Adv. Cancer Res.* **117:** 201–235.
2. Maceyka, M., K. B. Harikumar, S. Milstien, and S. Spiegel. 2012. Sphingosine-1-phosphate signaling and its role in disease. *Trends Cell Biol.* **22:** 50–60.
3. Snider, A. J., K. A. Orr Gandy, and L. M. Obeid. 2010. Sphingosine kinase: role in regulation of bioactive sphingolipid mediators in inflammation. *Biochimie.* **92:** 707–715.
4. Chi, H. 2011. Sphingosine-1-phosphate and immune regulation: trafficking and beyond. *Trends Pharmacol. Sci.* **32:** 16–24.
5. Yanagida, K., and T. Hla. 2017. Vascular and immunobiology of the circulatory sphingosine 1-phosphate gradient. *Annu. Rev. Physiol.* **79:** 67–91.
6. Kawamori, T., W. Osta, K. R. Johnson, B. J. Pettus, J. Bielawski, T. Tanaka, M. J. Wargovich, B. S. Reddy, Y. A. Hannun, L. M. Obeid, et al. 2006. Sphingosine kinase 1 is up-regulated in colon carcinogenesis. *FASEB J.* **20:** 386–388.
7. Johnson, K. R., K. Y. Johnson, H. G. Crellin, B. Ogretmen, A. M. Boylan, R. A. Harley, and L. M. Obeid. 2005. Immunohistochemical distribution of sphingosine kinase 1 in normal and tumor lung tissue. *J. Histochem. Cytochem.* **53:** 1159–1166.
8. Salama, M. F., B. Carroll, M. Adada, M. Pulkoski-Gross, Y. A. Hannun, and L. M. Obeid. 2015. A novel role of sphingosine kinase-1 in the invasion and angiogenesis of VHL mutant clear cell renal cell carcinoma. *FASEB J.* **29:** 2803–2813.
9. Van Brocklyn, J. R., C. A. Jackson, D. K. Pearl, M. S. Kotur, P. J. Snyder, and T. W. Prior. 2005. Sphingosine kinase-1 expression correlates with poor survival of patients with glioblastoma multiforme: roles of sphingosine kinase isoforms in growth of glioblastoma cell lines. *J. Neuropathol. Exp. Neurol.* **64:** 695–705.
10. Ohotski, J., J. S. Long, C. Orange, B. Elsberger, E. Mallon, J. Doughty, S. Pyne, N. J. Pyne, and J. Edwards. 2012. Expression of sphingosine 1-phosphate receptor 4 and sphingosine kinase 1 is associated with outcome in oestrogen receptor-negative breast cancer. *Br. J. Cancer.* **106:** 1453–1459.
11. Cai, H., X. Xie, L. Ji, X. Ruan, and Z. Zheng. 2017. Sphingosine kinase 1: A novel independent prognosis biomarker in hepatocellular carcinoma. *Oncol. Lett.* **13:** 2316–2322.
12. Akao, Y., Y. Banno, Y. Nakagawa, N. Hasegawa, T. J. Kim, T. Murate, Y. Igarashi, and Y. Nozawa. 2006. High expression of sphingosine kinase 1 and S1P receptors in chemotherapy-resistant prostate cancer PC3 cells and their camptothecin-induced up-regulation. *Biochem. Biophys. Res. Commun.* **342:** 1284–1290.
13. Gao, H., and L. Deng. 2014. Sphingosine kinase-1 activation causes acquired resistance against Sunitinib in renal cell carcinoma cells. *Cell Biochem. Biophys.* **68:** 419–425.
14. Olivera, A., T. Kohama, L. C. Edsall, V. E. Nava, O. Cuvillier, S. Poulton, and S. Spiegel. 1999. Sphingosine kinase expression increases intracellular sphingosine 1 phosphate and promotes cell growth and survival. *J. Cell Biol.* **147:** 545–558.
15. Snider, A. J., T. Kawamori, S. G. Bradshaw, K. A. Orr, G. S. Gilkeson, Y. A. Hannun, and L. M. Obeid. 2009. A role for sphingosine kinase 1 in dextran sulfate sodium-induced colitis. *FASEB J.* **23:** 143–152.
16. Snider, A. J., W. H. Ali, J. A. Sticca, N. Coant, A. M. Ghaleb, T. Kawamori, V. W. Yang, Y. A. Hannun, and L. M. Obeid. 2014. Distinct roles for hematopoietic and extra-hematopoietic sphingosine kinase-1 in inflammatory bowel disease. *PLoS One.* **9:** e113998.
17. Johnson, K. R., K. P. Becker, M. M. Facchinetti, Y. A. Hannun, and L. M. Obeid. 2002. PKC-dependent activation of sphingosine kinase 1 and translocation to the plasma membrane. Extracellular release of sphingosine-1-phosphate induced by phorbol 12-myristate 13-acetate (PMA). *J. Biol. Chem.* **277:** 35257–35262.
18. Sutherland, C. M., P. A. Moretti, N. M. Hewitt, C. J. Bagley, M. A. Vadas, and S. M. Pitson. 2006. The calmodulin-binding site of sphingosine kinase and its role in agonist-dependent translocation of sphingosine kinase 1 to the plasma membrane. *J. Biol. Chem.* **281:** 11693–11701.
19. Pitson, S. M., P. A. Moretti, J. R. Zebol, H. E. Lynn, P. Xia, M. Vadas, and B. W. Wattenberg. 2003. Activation of sphingosine kinase 1 by ERK1/2-mediated phosphorylation. *EMBO J.* **22:** 5491–5500.
20. Olivera, A., J. Rosenthal, and S. Spiegel. 1996. Effects of acidic phospholipids on sphingosine kinase. *J. Cell. Biochem.* **60:** 529–537.
21. Stahelin, R. V., J. H. Hwang, J. H. Kim, Z. Y. Park, K. R. Johnson, L. M. Obeid, and W. Cho. 2005. The mechanism of membrane targeting of human sphingosine kinase 1. *J. Biol. Chem.* **280:** 43030–43038.
22. Delon, C., M. Manifava, E. Wood, D. Thompson, S. Krugmann, S. Pyne, and N. T. Ktistakis. 2004. Sphingosine kinase 1 is an intracellular effector of phosphatidic acid. *J. Biol. Chem.* **279:** 44763–44774.
23. Shen, H., F. Giordano, Y. Wu, J. Chan, C. Zhu, I. Milosevic, X. Wu, K. Yao, B. Chen, T. Baumgart, et al. 2014. Coupling between endocytosis and sphingosine kinase 1 recruitment. *Nat. Cell Biol.* **16:** 652–662.
24. Jarman, K. E., P. A. Moretti, J. R. Zebol, and S. M. Pitson. 2010. Translocation of sphingosine kinase 1 to the plasma membrane is mediated by calcium- and integrin-binding protein 1. *J. Biol. Chem.* **285:** 483–492.
25. Zhu, W., B. L. Gliddon, K. E. Jarman, P. A. B. Moretti, T. Tin, L. V. Parise, J. M. Woodcock, J. A. Powell, A. Ruszkiewicz, M. R. Pitman, et al. 2017. CIB1 contributes to oncogenic signalling by Ras via modulating the subcellular localisation of sphingosine kinase 1. *Oncogene.* **36:** 2619–2627.
26. Pettersen, E. F., T. D. Goddard, C. C. Huang, G. S. Couch, D. M. Greenblatt, E. C. Meng, and T. E. Ferrin. 2004. UCSF Chimera–a visualization system for exploratory research and analysis. *J. Comput. Chem.* **25:** 1605–1612.
27. Dolinsky, T. J., J. E. Nielsen, J. A. McCammon, and N. A. Baker. 2004. PDB2PQR: an automated pipeline for the setup of Poisson-Boltzmann electrostatics calculations. *Nucleic Acids Res.* **32:** W665–W667.
28. Dolinsky, T. J., P. Czodrowski, H. Li, J. E. Nielsen, J. H. Jensen, G. Klebe, and N. A. Baker. 2007. PDB2PQR: expanding and upgrading automated preparation of biomolecular structures for molecular simulations. *Nucleic Acids Res.* **35:** W522–W525.
29. Baker, N. A., D. Sept, S. Joseph, M. J. Holst, and J. A. McCammon. 2001. Electrostatics of nanosystems: application to microtubules and the ribosome. *Proc. Natl. Acad. Sci. USA.* **98:** 10037–10041.
30. Kyte, J., and R. F. Doolittle. 1982. A simple method for displaying the hydropathic character of a protein. *J. Mol. Biol.* **157:** 105–132.
31. Billich, A., and P. Ettmayer. 2004. Fluorescence-based assay of sphingosine kinases. *Anal. Biochem.* **326:** 114–119.
32. Adada, M. M., D. Canals, N. Jeong, A. D. Kelkar, M. Hernandez-Corbacho, M. J. Pulkoski-Gross, J. C. Donaldson, Y. A. Hannun, and L. M. Obeid. 2015. Intracellular sphingosine kinase 2-derived sphingosine-1-phosphate mediates epidermal growth factor-induced ezrin-radixin-moesin phosphorylation and cancer cell invasion. *FASEB J.* **29:** 4654–4669.
33. Papahadjopoulos, D., and N. Miller. 1967. Phospholipid model membranes. I. Structural characteristics of hydrated liquid crystals. *Biochim. Biophys. Acta.* **135:** 624–638.
34. Sanjana, N. E., O. Shalem, and F. Zhang. 2014. Improved vectors and genome-wide libraries for CRISPR screening. *Nat. Methods.* **11:** 783–784.
35. Shalem, O., N. E. Sanjana, E. Hartenian, X. Shi, D. A. Scott, T. Mikkelson, D. Heckl, B. L. Ebert, D. E. Root, J. G. Doench, et al. 2014. Genome-scale CRISPR-Cas9 knockout screening in human cells. *Science.* **343:** 84–87.
36. Spassieva, S., J. Bielawski, V. Anelli, and L. M. Obeid. 2007. Combination of C(17) sphingoid base homologues and mass spectrometry analysis as a new approach to study sphingolipid metabolism. *Methods Enzymol.* **434:** 233–241.
37. Vadas, O., M. L. Jenkins, G. L. Dornan, and J. E. Burke. 2017. Using hydrogen-deuterium exchange mass spectrometry to examine protein-membrane interactions. *Methods Enzymol.* **583:** 143–172.
38. Wang, Z., X. Min, S. H. Xiao, S. Johnstone, W. Romanow, D. Meininger, H. Xu, J. Liu, J. Dai, S. An, et al. 2013. Molecular basis of sphingosine kinase 1 substrate recognition and catalysis. *Structure.* **21:** 798–809.
39. Dornan, G. L., B. D. Siempelkamp, M. L. Jenkins, O. Vadas, C. L. Lucas, and J. E. Burke. 2017. Conformational disruption of PI3Kdelta regulation by immunodeficiency mutations in PIK3CD and PIK3R1. *Proc. Natl. Acad. Sci. USA.* **114:** 1982–1987.
40. Siempelkamp, B. D., M. K. Rathinaswamy, M. L. Jenkins, and J. E. Burke. 2017. Molecular mechanism of activation of class IA phosphoinositide 3-kinases (PI3Ks) by membrane-localized HRas. *J. Biol. Chem.* **292:** 12256–12266.
41. Masson, G. R., O. Perisic, J. E. Burke, and R. L. Williams. 2016. The intrinsically disordered tails of PTEN and PTEN-L have distinct roles in regulating substrate specificity and membrane activity. *Biochem. J.* **473:** 135–144.

42. Vadas, O., and J. E. Burke. 2015. Probing the dynamic regulation of peripheral membrane proteins using hydrogen deuterium exchange-MS (HDX-MS). *Biochem. Soc. Trans.* **43:** 773–786.
43. Adams, D. R., S. Pyne, and N. J. Pyne. 2016. Sphingosine kinases: emerging structure-function insights. *Trends Biochem. Sci.* **41:** 395–409.
44. Gandy, K. A., D. Canals, M. Adada, M. Wada, P. Roddy, A. J. Snider, Y. A. Hannun, and L. M. Obeid. 2013. Sphingosine 1-phosphate induces filopodia formation through S1PR2 activation of ERM proteins. *Biochem. J.* **449:** 661–672.
45. Mizugishi, K., T. Yamashita, A. Olivera, G. F. Miller, S. Spiegel, and R. L. Proia. 2005. Essential role for sphingosine kinases in neural and vascular development. *Mol. Cell. Biol.* **25:** 11113–11121.
46. Barr, R. K., H. E. Lynn, P. A. Moretti, Y. Khew-Goodall, and S. M. Pitson. 2008. Deactivation of sphingosine kinase 1 by protein phosphatase 2A. *J. Biol. Chem.* **283:** 34994–35002.
47. Pitman, M. R., R. K. Barr, B. L. Gliddon, A. M. Magarey, P. A. Moretti, and S. M. Pitson. 2011. A critical role for the protein phosphatase 2A B'alpha regulatory subunit in dephosphorylation of sphingosine kinase 1. *Int. J. Biochem. Cell Biol.* **43:** 342–347.
48. Bayraktar, O., E. Ozkirimli, and K. Ulgen. 2017. Sphingosine kinase 1 (SK1) allosteric inhibitors that target the dimerization site. *Comput. Biol. Chem.* **69:** 64–76.
49. Siow, D. L., C. D. Anderson, E. V. Berdyshev, A. Skobeleva, S. M. Pitson, and B. W. Wattenberg. 2010. Intracellular localization of sphingosine kinase 1 alters access to substrate pools but does not affect the degradative fate of sphingosine-1-phosphate. *J. Lipid Res.* **51:** 2546–2559.
50. Safadi-Chamberlain, F., L. P. Wang, S. G. Payne, C. U. Lim, S. Stratford, J. A. Chavez, M. H. Fox, S. Spiegel, and S. A. Summers. 2005. Effect of a membrane-targeted sphingosine kinase 1 on cell proliferation and survival. *Biochem. J.* **388:** 827–834.
51. Hengst, J. A., J. M. Guilford, E. J. Conroy, X. Wang, and J. K. Yun. 2010. Enhancement of sphingosine kinase 1 catalytic activity by deletion of 21 amino acids from the COOH-terminus. *Arch. Biochem. Biophys.* **494:** 23–31.
52. Taha, T. A., Y. A. Hannun, and L. M. Obeid. 2006. Sphingosine kinase: biochemical and cellular regulation and role in disease. *J. Biochem. Mol. Biol.* **39:** 113–131.
53. Hannun, Y. A., and L. M. Obeid. 2008. Principles of bioactive lipid signalling: lessons from sphingolipids. *Nat. Rev. Mol. Cell Biol.* **9:** 139–150.
54. Spiegel, S., and S. Milstien. 2003. Sphingosine-1-phosphate: an enigmatic signalling lipid. *Nat. Rev. Mol. Cell Biol.* **4:** 397–407.
55. Guo, L., G. Mishra, K. Taylor, and X. Wang. 2011. Phosphatidic acid binds and stimulates Arabidopsis sphingosine kinases. *J. Biol. Chem.* **286:** 13336–13345.
56. Lee, Y. H., H. S. Kim, J. K. Pai, S. H. Ryu, and P. G. Suh. 1994. Activation of phospholipase D induced by platelet-derived growth factor is dependent upon the level of phospholipase C-gamma 1. *J. Biol. Chem.* **269:** 26842–26847.
57. Yeo, E. J., and J. H. Exton. 1995. Stimulation of phospholipase D by epidermal growth factor requires protein kinase C activation in Swiss 3T3 cells. *J. Biol. Chem.* **270:** 3980–3988.
58. Balboa, M. A., B. L. Firestein, C. Godson, K. S. Bell, and P. A. Insel. 1994. Protein kinase C alpha mediates phospholipase D activation by nucleotides and phorbol ester in Madin-Darby canine kidney cells. Stimulation of phospholipase D is independent of activation of polyphosphoinositide-specific phospholipase C and phospholipase A2. *J. Biol. Chem.* **269:** 10511–10516.
59. Paugh, B. S., S. W. Paugh, L. Bryan, D. Kapitonov, K. M. Wilczynska, S. M. Gopalan, H. Rokita, S. Milstien, S. Spiegel, and T. Kordula. 2008. EGF regulates plasminogen activator inhibitor-1 (PAI-1) by a pathway involving c-Src, PKCdelta, and sphingosine kinase 1 in glioblastoma cells. *FASEB J.* **22:** 455–465.
60. Nincheri, P., C. Bernacchioni, F. Cencetti, C. Donati, and P. Bruni. 2010. Sphingosine kinase-1/S1P1 signalling axis negatively regulates mitogenic response elicited by PDGF in mouse myoblasts. *Cell. Signal.* **22:** 1688–1699.
61. Donaldson, J. G. 2009. Phospholipase D in endocytosis and endosomal recycling pathways. *Biochim. Biophys. Acta.* **1791:** 845–849.